

EFFICIENT CHARGE CARRIER EXTRACTION IN PEROVSKITE-SILICON TANDEM SOLAR CELLS INVESTIGATED BY NUMERICAL SIMULATION

Christoph Messmer^{1,2}, Jonas Schön^{1,2}, Uli Würfel^{2,3}, Patricia S. C. Schulze², Martin C. Schubert², Martin Bivour²,
Stefan W. Glunz^{1,2}, Martin Hermle²

¹ INATECH, University of Freiburg, Emmy-Noether-Str. 2, 79110 Freiburg, Germany

² Fraunhofer Institute for Solar Energy Systems ISE, Heidenhofstr. 2, 79110 Freiburg, Germany

³ Materials Research Center FMF, University of Freiburg, Stefan-Meier-Str. 21, 79104 Freiburg, Germany

ABSTRACT: This work presents a comprehensive opto-electrical simulation model in Sentaurus TCAD for perovskite-silicon tandem devices which incorporates sophisticated physical models that allow for an in-depth study of efficient charge carrier extraction in tandem devices.

Keywords: photovoltaics, perovskite-silicon tandem solar cells, simulation

1 INTRODUCTION

Perovskite-silicon tandem devices exceeded the 30% efficiency threshold in laboratory [1] and are supposed to be suitable for low-cost mass-production in the near future [2, 3]. Besides the experimentally remarkable success within the last years, the main focus of simulation work was put into optical modelling, whereas electrical modelling somewhat lagged behind. However, electrical modeling could play an important role in understanding and systematically reducing the limitations in current tandem solar cells.

The aim of this and future work is to understand the present limitations of recently published tandem devices and to help overcoming the limitations by discrete guidelines which boost the tandem efficiency.

2 SIMULATION MODEL

We elaborated a full opto-electrical simulation model in Sentaurus TCAD [5] that is capable to describe state-of-the-art perovskite-silicon tandem solar cells [4, 6]. Figure 1 shows the full layer stack of the perovskite-silicon tandem device. The bottom cell is a silicon heterojunction (SHJ) with textured rear side. The planar front side features the a-Si electron contact followed by the ITO recombination junction towards the top cell's hole

transport layer (HTL) which is made up of a 1-nm-thick 2PACz layer acting as self-assembled monolayer. The top cell is featuring a triple cation perovskite absorber with a C₆₀/SnO_x stack as electron transport layer (ETL) that is followed by an ITO for lateral conductance towards the silver fingers. The MgF₂ layer is used to minimize the reflection of the device.

Optical modelling is performed using raytracing in crystalline silicon and transfer-matrix-method (TMM) for the top and bottom cell thin-film layer stacks (including the perovskite absorber), which was experimentally validated in a previous publication [2] for the 25.1%-efficient perovskite-silicon tandem cell of Schulze *et al.* [6]. The optical model was used to improve the tandem devices by a proposed optical roadmap which was capable to describe the most recently published perovskite-silicon tandem device by Heydarian *et al.* [4].

The electrical model for the silicon bottom cell and tunneling at the TCO recombination junction is used as published in several previous publications [2, 7]. The innovation of this paper is the extension of electrical model of the perovskite top cell including all relevant layers shown in Figure 1. It includes a drift-diffusion model for the mobile anions and cations within the perovskite absorber and allows for an in-depth study of the charge-carrier extraction at the electron and hole transport layer (in this study: C₆₀ and 2PACz, respectively) of the perovs-



Figure 1: Layer stack of the perovskite-silicon tandem solar cell as published in [4].

kite top cell.

3 RESULTS

3.1 Investigation of efficient charge carrier extraction

Requirements for efficient charge carrier extraction at the top cell's electron and hole contact layers are investigated by assessing the band diagrams of the perovskite-silicon tandem device as shown in Figure 2. Figure 2(a) shows the band diagram at open-circuit conditions V_{oc} . One can see that $\text{SnO}_x/\text{C}_{60}$ /perovskite interface at which efficient electron extraction is required. The parameters of the C_{60} and perovskite were chosen according to measurements following the publication of [8]. At the C_{60} /perovskite interface, the high non-radiative recombination reported in literature [4, 8] is accounted for by Shockley-Read-Hall recombination varying the hole recombination velocity $S_{0,h}^{\text{ETL}}$ (shown in gray) at this interface. One can see that for very high $S_{0,h}^{\text{ETL}}$, that the internal voltage of the perovskite top cell iV_{oc}^{Pero} drops significantly revealing a passivation loss. Furthermore, the Quasi-Fermi level of the electrons shows a significant drop towards the ETL/Pero interface which is highlighted in Figure 2b as ΔV_{oc} , revealing further extraction losses due to the highly recombination active ETL/Pero interface.

The hole extraction of the top cell 2PACz layer was modelled by a 1-nm-thick layer with dipole moment of $5 \cdot 10^{13} \text{ cm}^{-2}$ which effectively changes the ITO work function WF_{ITO} (from around 4.8 eV to 5.4 eV according to [9]) facilitating the hole extraction. The 2PACz/ITO junction allows for band-to-band tunneling of holes from the 2PACz side with electrons from the ITO side which electrically interconnects the top and bottom cell of the tandem device. Figure 2a also shows the electron contact of the silicon bottom cell featuring amorphous silicon (i.e. an a-Si(i)/a-Si(n) stack). Electron tunneling at the a-Si(n)/ITO barrier is accounted for in the model.

The anion and cation density within the perovskite top cell is shown in Figure 2 in green and light blue, respectively (see right axis). For the negatively charged anions, a diffusion coefficient of $1 \cdot 10^{-12} \text{ cm}^2/\text{s}$ was assumed whereas the diffusion coefficient of the positively charged cations is assumed to be one order of magnitude lower

according to measurement reported in literature concerning triple cation perovskites [10]. In quasi-steady state (i.e. holding the transient simulations sufficiently long) the negatively charged anions accumulate at the ETL (shown in green), whereas the positively charged cations accumulate at the HTL (shown in blue). This increases the requirements on efficient charge carrier extraction since anions and electrons (cations and holes) compete at the ETL (HTL) interface.

Figure 2b shows the band diagram at short-circuit conditions j_{sc} (i.e., at zero voltage) after a 90 second long transient sweep from V_{oc} (Figure 2a). One can see that the distribution of the less mobile cations barely changed with respect to Figure 2a, whereas the mobile anions moved further towards the ETL due to the electric field within the perovskite absorber. The higher anion concentration at the ETL/Pero interface and lower anion concentration at the Pero/HTL interface raises the requirements for efficient electron and hole extraction at the respective interfaces which is typically visible in the forward scan from j_{sc} to V_{oc} (shown in the next subsection).

3.2 Influence on the JV parameters

Figure 3 shows the simulated transient JV curves of the bottom (red), top (blue) and tandem device (green) for the reverse (i.e., V_{oc} to j_{sc} , solid line) (i.e., j_{sc} to V_{oc} , dashed line), respectively. One can see a high current density of about $19.6 \text{ mA}/\text{cm}^2$ of the current-matched device according to the experimental devices presented by Heydarian *et al.* [4]. The hysteresis of the perovskite top cell (i.e., difference between reverse and forward scan) is almost negligible which is in line with [4]. However, the potential of more efficient charge carrier extraction can be visualized by plotting the internal voltage curves (see dotted lines for perovskite top cell and tandem device). At V_{oc} , the difference ΔV_{oc} between the internal voltage iV_{oc} and external voltage is shown (orange). This can be attributed to the high SRH recombination at the ETL/Pero interface which is currently being investigated to further improve the electron extraction at this interface. At the MPP the ΔV_{mpp} . Here, a reduction of the effective series resistance of the device and more selective ETL and HTL layers could further improve the charge carrier extraction which is subject to future research.

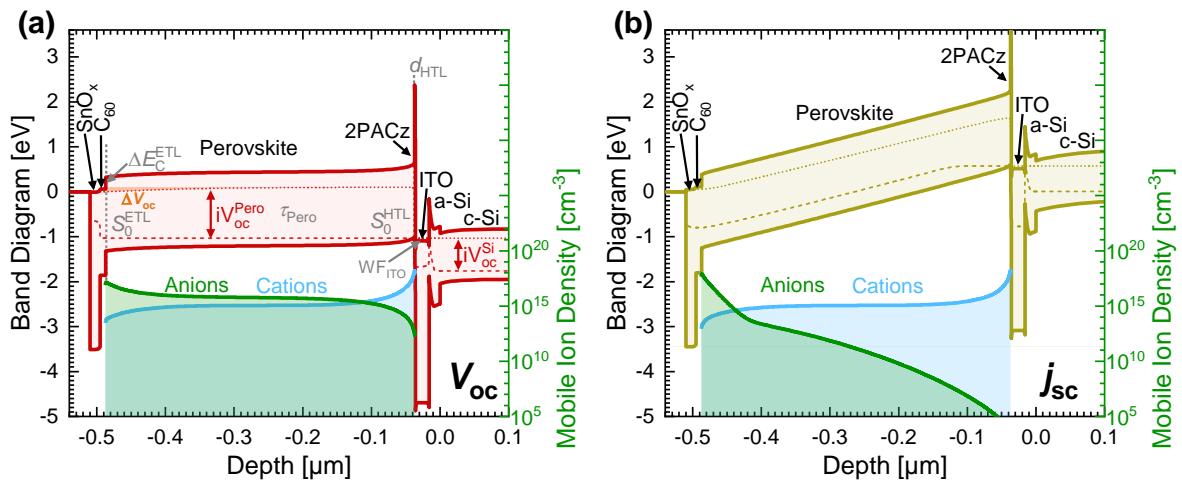


Figure 2: (a) Band diagram at V_{oc} (b) at j_{sc} . Right axis shows the density of mobile anions and cations within the perovskite absorber.

4 CONCLUSION

In this work, we presented a full opto-electrical simulation model in Sentaurus TCAD which incorporates sophisticated physical models to investigate the charge carrier extraction in perovskite-silicon tandem cells. This comprehensive model allows investigate the charge carrier transport in perovskite-silicon tandem devices and to assess the opto-electrical properties of the device including band diagrams and the transient JV sweeps including migration of anions and cations within the perovskite absorber. It will be applied in future works to interpret experimentally observed research topics and will be further used to optimize perovskite-silicon tandem devices for higher efficiency and stability.

5 ACKNOWLEDGEMENTS

This work was supported by the German Federal Ministry of Economic Affairs and Climate Action within the research projects “KATANA” (contract number 03EE1087A and 03EE1087B) and “PrEsto” (contract number 03EE1086A) and the Fraunhofer LIGHTHOUSE PROJECT (MaNiTU).

6 REFERENCES

- [1] EPFL, *New world records: perovskite-on-silicon-tandem solar cells: EPFL and CSEM smash through the 30% efficiency barrier for perovskite-on-silicon-tandem solar cells—setting two certified world records.*, 2022.
- [2] C. Messmer, B. S. Goraya, S. Nold, P. S. Schulze, V. Sittinger, J. Schön, J. C. Goldschmidt, M. Bivour, S. W. Glunz, and M. Hermle, “The race for the best silicon bottom cell: Efficiency and cost evaluation of perovskite–silicon tandem solar cells,” *Prog. Photovolt: Res. Appl.*, vol. 29, no. 7, pp. 744–759, 2021.
- [3] L. A. Zafoschnig, S. Nold, and J. C. Goldschmidt, “The race for lowest costs of electricity production: techno-economic analysis of silicon, perovskite and tandem solar cells,” *IEEE Journal of Photovoltaics*, vol. 10, no. 6, pp. 1632–1641, 2020.
- [4] M. Heydarian, C. Messmer, A. J. Bett, M. Heydarian, D. Chojniak, Ö. S. Kabakli, L. Tutsch, M. Bivour, F. Schindler, G. Siefer, M. C. Schubert, J. C. Goldschmidt, M. Hermle, S. W. Glunz, and P. S. Schulze, “Maximizing Current Density in Monolithic Perovskite Silicon Tandem Solar Cells,” *Solar RRL*.
- [5] Synopsis, “Sentaurus TCAD: Release Q-2019.12,” <http://www.synopsys.com>, 2019.
- [6] P. S. C. Schulze, A. J. Bett, M. Bivour, P. Caprioglio, F. M. Gerspacher, Ö. Ş. Kabakli, A. Richter, M. Stolterfoht, Q. Zhang, D. Neher, M. Hermle, H. Hillebrecht, S. W. Glunz, and J. C. Goldschmidt, “25.1% High-Efficiency Monolithic Perovskite Silicon Tandem Solar Cell with a High Bandgap Perovskite Absorber,” *Sol. RRL*, vol. 4, no. 7, p. 2000152, 2020.
- [7] C. Messmer, J. Schön, S. Lohmüller, J. Greulich, C. Luderer, J. C. Goldschmidt, M. Bivour, S. W. Glunz, and M. Hermle, “How to make PERC suitable for perovskite–silicon tandem solar cells: A simulation study,” *Prog. Photovolt: Res. Appl.*, <https://onlinelibrary.wiley.com/doi/full/10.1002/pi.p.3524>, 2022.
- [8] D. Menzel, A. Al-Ashouri, A. Tejada, I. Levine, J. A. Guerra, B. Rech, S. Albrecht, and L. Korte, “Field Effect Passivation in Perovskite Solar Cells by a LiF Interlayer,” *Advanced Energy Materials*, p. 2201109, 2022.
- [9] J. Hu, W. Fu, X. Yang, and H. Chen, “Self-assembled monolayers for interface engineering in polymer solar cells,” *Journal of Polymer Science*, 2022.
- [10] B. Li, C. Kan, P. Hang, Y. Fang, L. Zuo, L. Song, Y. Zhang, D. Yang, and X. Yu, “Understanding the Influence of Cation and Anion Migration on Mixed-Composition Perovskite Solar Cells via Transient Ion Drift,” *Physica Rapid Research Ltrs*, vol. 15, no. 9, p. 2100225, 2021.

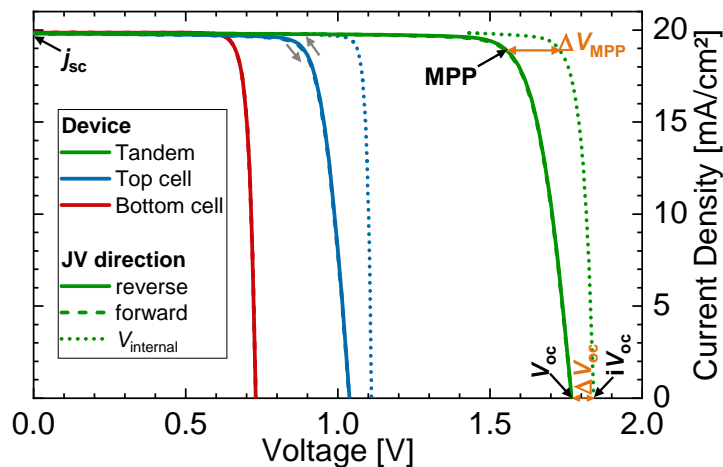


Figure 3: Simulated JV curves of top (blue), bottom (red) and tandem (green) solar cell for reverse and forward scan as solid and dashed curves, respectively. The dotted curves show the internal voltage curves (i.e., the current density versus the averaged Quasi-Fermi level splitting within the respective absorber(s))